

Finite element solution of Laplace's equation for ion-atom chambers

Jacob Golde, Janine Shertzer, and Paul Oxley

Department of Physics, College of the Holy Cross, Worcester, Massachusetts 01610

(Received 18 July 2008; accepted 23 September 2008)

The finite element method is used to solve Laplace's equation for ion-atom chambers. We first consider a simplified model chamber for which an analytical solution can be obtained; the model chamber serves as a test case to verify the accuracy and convergence of the finite element method. We apply the finite element method to an experimental chamber consisting of five equipotential rings in a grounded cylindrical shell. We determine the strength and homogeneity of the electric field in the region of the chamber where the atoms undergo laser excitation into a Rydberg state. © 2009

American Association of Physics Teachers.

[DOI: 10.1119/1.3000255]

I. INTRODUCTION

A wide range of atomic physics experiments are done in external static electric fields. Calculating the electric field generated by a particular arrangement of electrical conductors is critical for designing successful experiments and interpreting experimental data. Here we focus on collision experiments involving Rydberg atoms¹ in a specially prepared atomic state. The excitation of the atoms and the subsequent collision with ions is carried out in an ion-atom chamber. The atomic beam first passes through a region of the chamber where the atoms undergo laser excitation into a Rydberg state in the presence of a strong electric field. The field must be very homogeneous, otherwise the atomic energy levels are shifted out of resonance with the laser and excitation cannot occur. As the atomic beam travels down the ion-atom chamber, the electric field decreases in magnitude and the atoms evolve into a coherent elliptical state.^{2,3} The coherent elliptical state atoms then enter a second region where the electric field is weak but uniform; here the atoms undergo charge-transfer collisions with singly charged ions.^{4,5} The ion-atom chamber consists of a grounded cylindrical shell with a series of conducting rings. By adjusting the potential of the individual rings, the field strength and homogeneity in different regions of the chamber can be manipulated.

To predict the electric potential in the ion-atom chamber we need to solve Laplace's equation⁶ with the appropriate boundary conditions. This equation is exactly solvable only for the simplest geometries and boundary conditions. For a realistic chamber, the electric potential is obtained by a numerical solution. Although commercial software packages are available, they function as a "black box," and it is often difficult to incorporate the exact details of the experimental apparatus. Running the codes provides no physical insight into the essential physics.

We present here the basic theory needed to develop a simple finite element method⁷ code to solve Laplace's equation. Although our interest is in ion-atom chambers, the finite element method can be used to solve Laplace's equation for any application, including atom and ion traps.⁸ Any second-order differential equation that arises in electromagnetic theory or quantum mechanics^{9,10} (including eigenvalue problems) can be solved with the finite element method.

In Sec. II we consider a simplified model chamber with a single equipotential disk in a grounded cylinder. Laplace's equation can be solved analytically for this case. The model chamber serves as a test case for verifying the accuracy of the finite element method. In Sec. III we discuss the finite

element method. We first show how the method can be applied to a simple second-order differential equation in one variable. We then explain how to generalize the method to higher dimensions and describe the solution of Laplace's equation in cylindrical coordinates. In Sec. IV we present our results. For the model chamber we compare the exact electric potential with that obtained using the finite element method. We then present our results for an experimental chamber with five equipotential rings of finite thickness. Concluding remarks are given in Sec. V.

II. ANALYTICAL SOLUTION FOR THE MODEL ION-ATOM CHAMBER

For the simplified model chamber we use a grounded cylinder with closed ends of radius a and length l . The chamber contains a single equipotential disk of radius a (and negligible thickness) which is electrically insulated from the chamber wall. The disk divides the chamber into two regions, where $-l_1 \leq z \leq 0$ in region 1 and $0 \leq z \leq l_2$ in region 2 and $l = l_1 + l_2$ (see Fig. 1). We align the z -axis along the horizontal direction of the atomic beam.

To find the potential inside the chamber we solve Laplace's equation in cylindrical coordinates

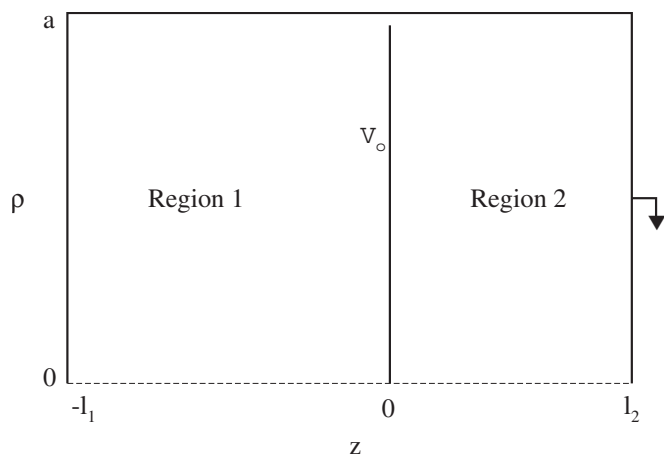


Fig. 1. The model chamber consists of a grounded closed cylindrical shell of radius a and length $l = l_1 + l_2$ with a single equipotential disk.

$$\left[\frac{\partial^2}{\partial \rho^2} + \frac{1}{\rho} \frac{\partial}{\partial \rho} + \frac{1}{\rho^2} \frac{\partial^2}{\partial \phi^2} + \frac{\partial^2}{\partial z^2} \right] V(\rho, \phi, z) = 0, \quad (1)$$

subject to the appropriate boundary conditions. Because of the azimuthal symmetry of the apparatus, there is no ϕ -dependence and $V(\rho, \phi, z) = V(\rho, z)$.

The general solution in both regions is given by

$$V(\rho, z) = [Ae^{kz} + Be^{-kz}]J_0(k\rho), \quad (2)$$

where $J_\nu(x)$ is the ν th order Bessel function.¹¹ In region 1 we impose the boundary condition $V(a, z) = V(\rho, -l_1) = 0$, and in region 2 we require that $V(a, z) = V(\rho, l_2) = 0$. We match the solutions at $z=0$ and require that $V(\rho, 0) = V_0$. If we use the orthogonality relation¹¹

$$\int_0^a J_\nu\left(\frac{\alpha_{v,m}\rho}{a}\right) J_\nu\left(\frac{\alpha_{v,n}\rho}{a}\right) \rho d\rho = \frac{a^2}{2} [J_{\nu+1}(\alpha_{v,n})]^2 \delta_{m,n}, \quad (3)$$

where $\alpha_{v,n}$ is the n th zero of $J_\nu(x)$, the potential in regions 1 and 2 is given by

$$V_1(\rho, z) = 2V_0 \sum_{n=1}^{\infty} \frac{J_0\left(\frac{\alpha_{0,n}\rho}{a}\right) \sinh\left[\frac{\alpha_{0,n}(l_1+z)}{a}\right]}{\alpha_{0,n} J_1(\alpha_{0,n}) \sinh\left[\frac{\alpha_{0,n}l_1}{a}\right]} (-l_1 \leq z \leq 0), \quad (4a)$$

$$V_2(\rho, z) = 2V_0 \sum_{n=1}^{\infty} \frac{J_0\left(\frac{\alpha_{0,n}\rho}{a}\right) \sinh\left[\frac{\alpha_{0,n}(l_2-z)}{a}\right]}{\alpha_{0,n} J_1(\alpha_{0,n}) \sinh\left[\frac{\alpha_{0,n}l_2}{a}\right]} (0 \leq z \leq l_2). \quad (4b)$$

The corresponding electric field $\vec{E} = -\vec{\nabla}V(\rho, z)$ is given by

$$\vec{E}_1(\rho, z) = \frac{2V_0}{a} \sum_{n=1}^{\infty} \frac{J_1\left(\frac{\alpha_{0,n}\rho}{a}\right) \sinh\left[\frac{\alpha_{0,n}(l_1+z)}{a}\right] \hat{\rho} - J_0\left(\frac{\alpha_{0,n}\rho}{a}\right) \cosh\left[\frac{\alpha_{0,n}(l_1+z)}{a}\right] \hat{z}}{J_1(\alpha_{0,n}) \sinh\left[\frac{\alpha_{0,n}l_1}{a}\right]}, \quad (5a)$$

$$\vec{E}_2(\rho, z) = \frac{2V_0}{a} \sum_{n=1}^{\infty} \frac{J_1\left(\frac{\alpha_{0,n}\rho}{a}\right) \sinh\left[\frac{\alpha_{0,n}(l_2-z)}{a}\right] \hat{\rho} + J_0\left(\frac{\alpha_{0,n}\rho}{a}\right) \cosh\left[\frac{\alpha_{0,n}(l_2-z)}{a}\right] \hat{z}}{J_1(\alpha_{0,n}) \sinh\left[\frac{\alpha_{0,n}l_2}{a}\right]}. \quad (5b)$$

The sum converges rapidly. Except in the immediate vicinity of the physical discontinuity at $\rho=a, z=0$ (where the equipotential disk is joined to the grounded cylinder), the potential and the electric field inside the chamber converge to eight or more significant digits with $n_{\max}=12$. (The values of $\alpha_{0,n}$ for $0 \leq n \leq 12$ are given in Ref. 12.)

III. FINITE ELEMENT METHOD

The finite element method⁷ is a numerical tool for solving second-order linear differential equations. It is ideally suited for solving problems with complex boundary conditions. In essence the method works by breaking up the continuum into small regions called elements. In each element we obtain a local solution to the differential equation by approximating the unknown function with a simple polynomial. The local solutions are then joined smoothly at the element boundaries. By systematically increasing the number of elements, we can obtain numerical results that converge to the desired accuracy.

We first apply the finite element method to a simple one-dimensional problem. Consider a linear second order differential equation

$$\frac{d^2f(x)}{dx^2} + xf(x) = 0 \quad (6)$$

on the range $[x_{\min}, x_{\max}]$. The function $f(x)$ is subject to the boundary conditions $f(x_{\min})=a$ and $f(x_{\max})=b$. In finite element analysis we subdivide the region $x_{\min} \leq x \leq x_{\max}$ into N elements, not necessarily of equal size. The midpoint of element n is $x_0^{(n)}$ and the width of the element is $2h^{(n)}$. Each element contains five equally spaced grid points, including the two end points, which are labeled $1 \leq i \leq 5$. There are a total of $4N+1$ grid points in the range $[x_{\min}, x_{\max}]$. The global index I of each grid point is related to the local index i in element n by

$$I = 4(n-1) + i. \quad (7)$$

In each element we introduce a local coordinate $-1 \leq x_l \leq 1$, which is related to the global coordinate x by

$$x = x_0^{(n)} + h^{(n)}x_l. \quad (8)$$

The five grid points are located at $x_l = -1, -1/2, 0, 1/2,$ and 1 . We approximate the function in element n as a linear combination of fourth degree polynomials $\phi_i(x_l)$,

Table I. The finite element basis functions which satisfy $\phi_j(-1 + \frac{1}{2}(j-1)) = \delta_{i,j}$.

$$\phi_1 = \frac{1}{6}x - \frac{1}{6}x^2 - \frac{2}{3}x^3 + \frac{2}{3}x^4$$

$$\phi_2 = -\frac{4}{3}x + \frac{8}{3}x^2 + \frac{4}{3}x^3 - \frac{8}{3}x^4$$

$$\phi_3 = 1 - 5x^2 + 4x^4$$

$$\phi_4 = \frac{4}{3}x + \frac{8}{3}x^2 - \frac{4}{3}x^3 - \frac{8}{3}x^4$$

$$\phi_5 = -\frac{1}{6}x - \frac{1}{6}x^2 + \frac{2}{3}x^3 + \frac{2}{3}x^4$$

$$f^{(n)}(x) = \sum_{j=1}^5 f_j^{(n)} \phi_j(x_i), \quad (9)$$

where $f_j^{(n)}$ is the yet undetermined expansion coefficient. The basis functions $\phi_j(x_i)$ are chosen such that $f_j^{(n)}$ is the numerical value of the function $f(x)$ at the j th grid point. The polynomial basis functions are completely determined by the requirement that

$$\phi_i\left(-1 + \frac{1}{2}(j-1)\right) = \delta_{i,j}. \quad (10)$$

The basis functions, which are independent of the element, are given in Table I.

If we substitute Eqs. (8) and (9) into Eq. (6), we obtain a differential equation in the local coordinate for element n ,

$$\sum_{j=1}^5 \left[\frac{1}{(h^{(n)})^2} \frac{d^2 \phi_j(x_l)}{dx_l^2} + (x_0^{(n)} + h^{(n)}x_l) \phi_j(x_l) \right] f_j^{(n)} = 0. \quad (11)$$

We then project Eq. (11) onto the basis functions $\phi_i(x_l)$ and integrate by parts. In matrix notation, we have

$$\sum_{j=1}^5 [S_{ij}^{(n)} + M_{ij}^{(n)}] f_j^{(n)} = 0, \quad (12)$$

where

$$S_{ij}^{(n)} = \delta_{i,5} \left. \frac{d\phi_j(x_l)}{h^{(n)} dx_l} \right|_{x_l=1} - \delta_{i,1} \left. \frac{d\phi_j(x_l)}{h^{(n)} dx_l} \right|_{x_l=-1}, \quad (13)$$

and

$$M_{ij}^{(n)} = \int_{-1}^1 \left[-\frac{d\phi_i(x_l)}{h^{(n)} dx_l} \frac{d\phi_j(x_l)}{h^{(n)} dx_l} + \phi_i(x_l)(x_0^{(n)} + h^{(n)}x_l) \phi_j(x_l) \right] h^{(n)} dx_l. \quad (14)$$

The matrix elements can be evaluated exactly because they are integrals of simple polynomials.

We now construct a global matrix by adding together the 5×5 local matrices for each element

$$\sum_{n=1}^N \sum_{j=1}^5 [S_{ij}^{(n)} + M_{ij}^{(n)}] f_j^{(n)} = \sum_{J=1}^{4N+1} [S_{IJ} + M_{IJ}] f_J = 0. \quad (15)$$

The global indices I, J are given by Eq. (7). Note that $f_{4n+1} = f_5^{(n)} = f_1^{(n+1)}$ for $1 \leq n < N$, which ensures continuity of the function across the element boundaries. The surface

terms from adjacent elements cancel, leaving only the contributions from the endpoints

$$S_{IJ} = \delta_{I,4N+1} \delta_{J,4(N-1)+j} \left. \frac{d\phi_j(x_l)}{h^{(N)} dx_l} \right|_{x_l=1} - \delta_{I,1} \delta_{J,j} \left. \frac{d\phi_j(x_l)}{h^{(1)} dx_l} \right|_{x_l=-1}. \quad (16)$$

We now impose the boundary conditions, which is equivalent to setting $f(x_{\min}) = f_1 = a$ and $f(x_{\max}) = f_{4N+1} = b$. We eliminate the rows of \mathbf{S} and \mathbf{M} corresponding to $I=1$ and $I=4N+1$. The eliminated rows associated with the boundary conditions are linear combinations of the remaining rows, consistent with the fact that $\det[\mathbf{S} + \mathbf{M}] = 0$.

The final equation which includes the boundary conditions is

$$\sum_{J=2}^{4N} M_{IJ} f_J = -M_{I1} a - M_{I(4N+1)} b \quad (I=2, \dots, 4N) \quad (17)$$

or $\tilde{\mathbf{M}}\mathbf{f} = \mathbf{x}$. The nonsingular matrix $\tilde{\mathbf{M}}$ is banded and symmetric, with a bandwidth of nine. The vector \mathbf{x} is mostly zeroes, because $M_{I1} = 0$, $I > 5$ and $M_{I(4N+1)} = 0$, $I < 4N-3$. The remaining $(4N-1)$ unknown components of \mathbf{f} can be obtained using a standard linear equation solver.

Equation (17) does not contain any of the tedious surface terms that were generated by the integration by parts. All the surface terms cancel, except at the endpoints, when the local matrices are added together. We eventually eliminate the first and last rows of the matrices \mathbf{S} and \mathbf{M} that correspond to the endpoints. In practice, we can simply ignore the surface terms and immediately construct the set of linear equations given in Eq. (17).

It is important to remember that although the unknown coefficients \mathbf{f} are the numerical value of the function at the grid points, the function is analytically determined in the range $[x_{\min}, x_{\max}]$. The piecewise continuous function $f(x)$ can be constructed using

$$f(x) = \sum_{n=1}^{4N+1} \sum_{j=1}^5 f_j^{(n)} \phi_j^{(n)}(x_l), \quad (18)$$

where $f_j^{(n)} = f_{4(n-1)+j}$.

Generalizing the finite element method to two dimensions is simple in theory. In practice, the bookkeeping becomes cumbersome, particularly when the boundary conditions are complicated. In this paper we seek a solution of Laplace's equation in cylindrical coordinates as given in Eq. (1). The two-dimensional continuum defined by $[z_{\min}, z_{\max}]$ and $[0, \rho_{\max}]$ is subdivided into $N = N_z N_\rho$ rectangular elements. The elements are numbered sequentially, with

$$n = N_z(n_\rho - 1) + n_z \quad (1 \leq n_z \leq N_z, 1 \leq n_\rho \leq N_\rho), \quad (19)$$

as shown in Fig. 2. The midpoint of each element is given by the coordinate $(z_0^{(n)}, \rho_0^{(n)})$ and the area of the rectangular element is $4h_z^{(n)} h_\rho^{(n)}$.

Each element contains a 5×5 array of equally spaced grid points (see Fig. 2). The local index associated with the grid point is

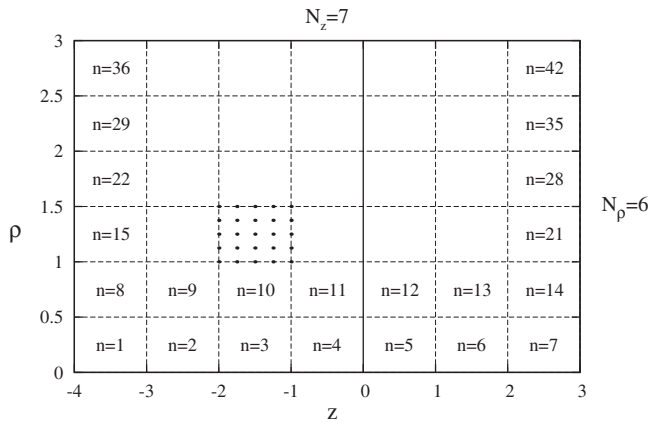


Fig. 2. The finite element grid for the model chamber. The chamber consists of a grounded closed cylindrical shell of radius $a=3$ and length $l=l_1+l_2$, where $l_1=4$ and $l_2=3$. The equipotential disk is held at $V_0=2$. The 25 local nodes are shown in element $n=17$.

$$i = 5(i_\rho - 1) + i_z \quad (1 \leq i_z \leq 5, 1 \leq i_\rho \leq 5). \quad (20)$$

The entire grid consists of $(4N_z+1)(4N_\rho+1)$ grid points. In element n the global index is related to the local index by

$$I = (4N_z + 1)[4(n_\rho - 1) + i_\rho - 1] + 4(n_z - 1) + i_z. \quad (21)$$

Again we introduce local coordinates $-1 \leq \rho_l \leq 1$ and $-1 \leq z_l \leq 1$ which are related to the global coordinates by

$$\rho = \rho_0^{(n)} + h_\rho^{(n)} \rho_l, \quad (22)$$

and

$$z = z_0^{(n)} + h_z^{(n)} z_l. \quad (23)$$

We expand the unknown function $V(\rho, z)$ into a linear combination of products of fourth degree polynomials in the two local coordinates

$$V(\rho, z) = \sum_{j_\rho=1}^5 \sum_{j_z=1}^5 V_j^{(n)} \phi_{j_z}(z_l) \phi_{j_\rho}(\rho_l), \quad (24)$$

The basis functions ϕ_j are given in Table I. We substitute Eq. (24) into Eq. (1) and project onto the basis functions to obtain a local matrix equation for element n ;

$$\begin{aligned} & \sum_{j_\rho=1}^5 \sum_{j_z=1}^5 \int_{-1}^{+1} \left[-\frac{d\phi_{j_\rho}(\rho_l)}{h_\rho^{(n)} d\rho_l} \frac{d\phi_{j_z}(z_l)}{h_z^{(n)} dz_l} \phi_{j_z}(z_l) \phi_{j_\rho}(\rho_l) \right. \\ & \left. - \phi_{j_\rho}(\rho_l) \phi_{j_z}(z_l) \frac{d\phi_{j_z}(z_l)}{h_z^{(n)} dz_l} \frac{d\phi_{j_\rho}(\rho_l)}{h_\rho^{(n)} d\rho_l} \right] h_z^{(n)} h_\rho^{(n)} \\ & \times (\rho_0^{(n)} + h_\rho^{(n)} \rho_l) d\rho_l dz_l V_j^{(n)} = 0. \end{aligned} \quad (25)$$

(We ignore the surface terms as explained previously.)

The 25×25 local matrices are then added together to form the global matrix; the local indices i, j are mapped into the global indices I, J using Eq. (21). This procedure ensures the continuity of the potential $V(\rho, z)$ across the element boundaries. Interior ‘‘edges’’ are shared by two elements and interior ‘‘corners’’ are shared by four elements. In two dimen-

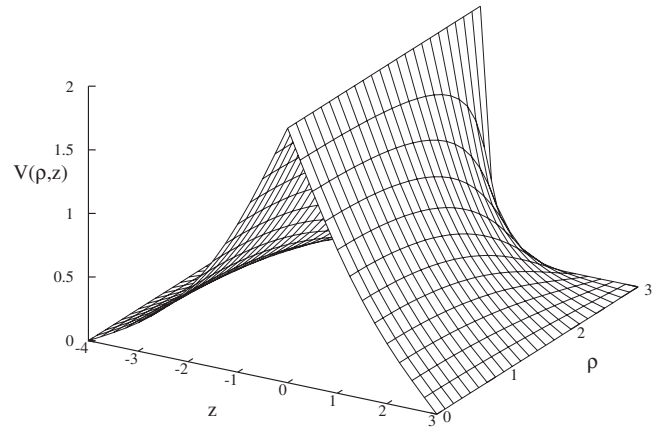


Fig. 3. The potential $V(\rho, z)$ inside the model chamber; the finite element method results are indistinguishable from the exact solution.

sions the global matrix has a multiple band structure, but is still symmetric. All the matrix elements can be calculated exactly.

Depending on the nature of the problem, the boundary conditions can be quite complicated. If the global component V_K corresponds to the known value of the potential on some boundary, then the K th row is eliminated from the global matrix and the product $M_{IK}V_K$ is carried over to the right-hand side, analogous to Eq. (17).

The boundary conditions for the model chamber are straightforward; the potential is zero along the grounded chamber walls and constant along the equipotential disk at $z=0$. For the experimental chamber special care must be taken to accommodate the multiple equipotential rings of finite thickness that are embedded inside the grounded chamber.

Once the remaining unknown components V_j are found, the piecewise continuous potential and electric field are given by

$$V(\rho, z) = \sum_{n=1}^N \sum_{j_\rho=1}^5 \sum_{j_z=1}^5 V_j^{(n)} \phi_{j_z}(z_l) \phi_{j_\rho}(\rho_l), \quad (26)$$

and

$$\begin{aligned} \vec{E}(\rho, z) = & - \sum_{n=1}^N \sum_{j_\rho=1}^5 \sum_{j_z=1}^5 V_j^{(n)} \left[\phi_{j_z}(z_l) \frac{d\phi_{j_\rho}(\rho_l)}{h_\rho^{(n)} d\rho_l} \hat{\rho} \right. \\ & \left. + \phi_{j_\rho}(\rho_l) \frac{d\phi_{j_z}(z_l)}{h_z^{(n)} dz_l} \hat{z} \right]. \end{aligned} \quad (27)$$

The derivative of the solution is not necessarily continuous across the element boundaries. However, as long as the potential is relatively smooth, the electric field is numerically continuous at the element boundaries (except at the edges of the equipotential rings).

IV. RESULTS

To test the finite element code and to establish the accuracy of the numerical solution we first compare the exact solution for the simplified model chamber with the finite element solution. In dimensionless units, we choose $a=3$, $l_1=4$, $l_2=3$, and $V_0=2$. We used a relatively crude grid with $N_z=7$ and $N_\rho=6$ for a total of 42 elements. It is important

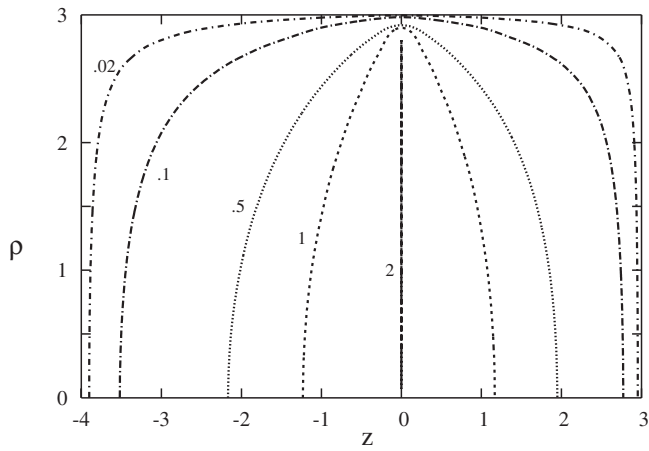


Fig. 4. The equipotential lines inside the model chamber.

that the equipotential disk is aligned with the edges of an element to accommodate the discontinuity in the electric field. The grid is superimposed over the chamber configuration in Fig. 2. To treat the unphysical discontinuity at $V(a,0)$, we require $V(\rho,0)=V_0$ except at $\rho=a$, where $V(a,0)=0$. The point discontinuity is smeared out over the distance between adjacent grid points. The results for the potential and the electric field agree with the exact solution to a few parts in 10^5 or better, except in a small region near the discontinuity. Greater accuracy could be achieved with more elements, but our goal was to show that even a relatively crude grid can yield accurate results for the single disk chamber. In Fig. 3 we show the potential surface for the simple model chamber. It is often more insightful to view the equipotential lines, which are shown in Fig. 4.

The experimental chamber consists of a grounded cylinder of radius 3.0 cm and length 7.1 cm. The chamber contains five equipotential rings with inner radius 0.25 cm and outer radius 2.0 cm; the rings are of finite thickness 0.20 cm. (The experimental chamber does not suffer from the unphysical discontinuity of the model chamber.) The five conducting rings were held at fixed potentials $-13.2, -12, 12, 13.2,$ and 13.8 V as shown in Fig. 5. The chamber was designed with the intent of creating a strong, highly uniform electric field in the region where the atoms are laser excited into a Rydberg state. The center of this region is midway between the -12 and 12 V rings at $z=3.2$ cm, where the electric field is about 20 V/cm. The center of this region is indicated with a dot on Fig. 5. Both the atomic beam and the laser beam are approximately 0.30 cm in width. The electric field needs to be uniform to within $\pm 0.1\%$ over a large part of the region where the atomic beam intersects the laser beam ($0 \leq \rho \leq 0.15$ cm, $3.05 \text{ cm} \leq z \leq 3.35$ cm). The ion-atom collisions occur in the second region midway between the 12 and 13.2 V rings at $z=4.6$ cm, where the field is weak (~ 1.0 V/cm) and uniform. The center of this region is also indicated with a dot on Fig. 5. The role of the first ring (-13.2 V) is to enhance the field homogeneity in the region of the laser excitation by “mirroring” the fourth ring. The role of the last ring (13.8 V) is to further shield the chamber interior from the electric fields outside the chamber that are used to analyze the exiting atomic beam.

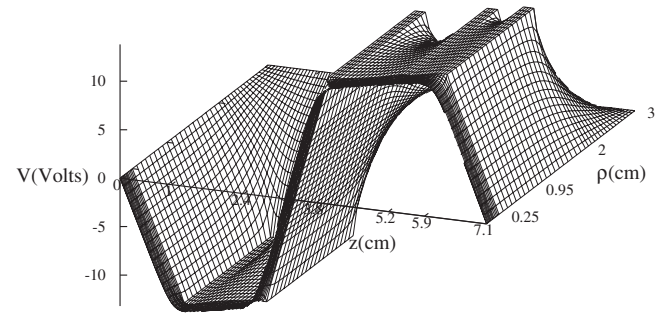


Fig. 6. The potential $V(\rho, z)$ inside the experimental chamber.

In Fig. 5 we show the final grid superimposed on the experimental chamber configuration. We systematically increased the number of elements, particularly in the region where the laser excitation occurs, until the results converged to sufficient accuracy to establish the homogeneity of the electric field to four significant digits. With $N_\rho=12$ and $N_z=29$, the total number of elements is 348. The equipotential rings are aligned with the edges of an element to accommodate the discontinuity in the derivative of the potential. After imposing the boundary conditions (including the cylinder

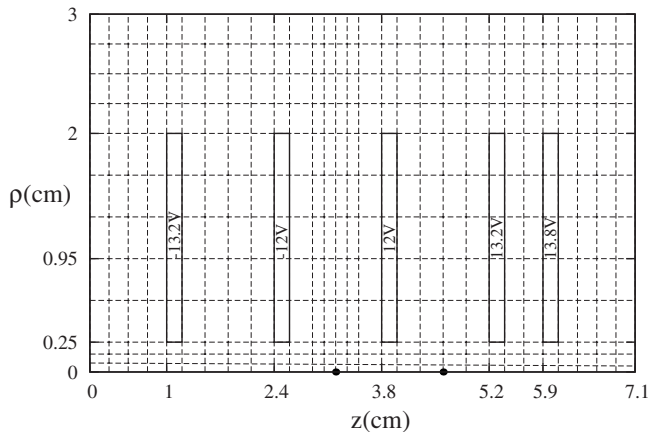


Fig. 5. The finite element grid for the experimental ion-atom chamber. The chamber consists of a grounded closed cylindrical shell with five equipotential rings of finite thickness. The two dots indicate the location of the laser excitation at $z=3.2$ cm (where the electric field is strong and highly uniform) and the site of the ion-atom collision at $z=4.6$ cm (where the electric field is weak and uniform).

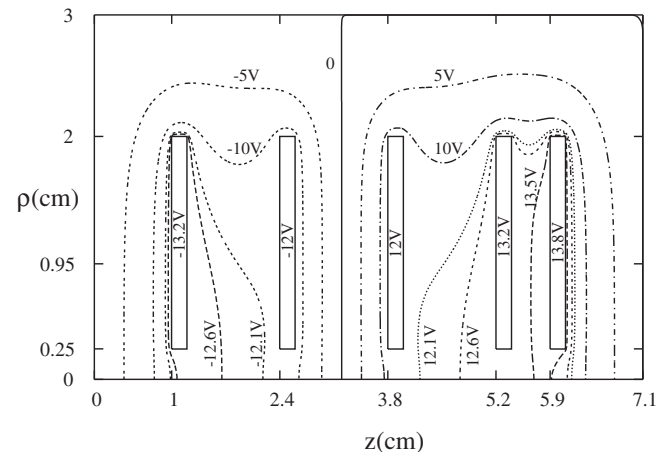


Fig. 7. The equipotential lines inside the experimental chamber.

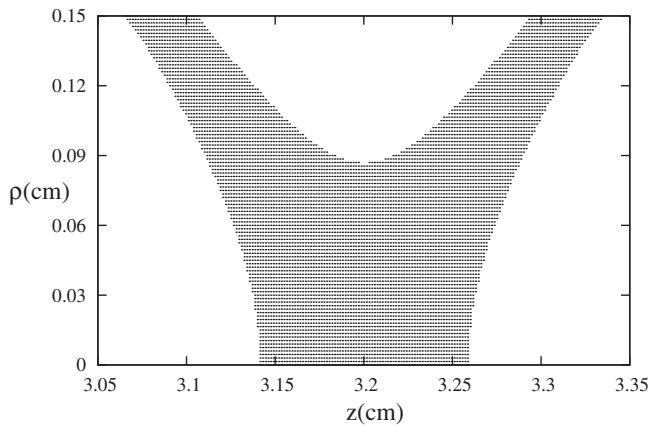


Fig. 8. The shaded region indicates the area inside the experimental chamber where $E(\rho, z) = E(0, 3.2 \text{ cm}) \pm 0.1\%$, which is the field homogeneity requirement for efficient laser excitation of the atoms.

walls and the five equipotential rings), the number of linear equations to be solved is 4995. Over 99% of the CPU time is spent in solving the final set of linear equations. Computational efficiency is improved by using an algorithm that exploits the symmetric nature of the matrix.

In Fig. 6 we show the potential surface for the experimental chamber; the corresponding equipotential lines inside the experimental chamber are shown in Fig. 7. We use Eq. (27) to determine the electric field in the region where the atoms are excited into Rydberg states. At the point where the center of the atomic beam intersects the center of the laser beam, the electric field is $\vec{E}(0, 3.2 \text{ cm}) = -19.545 \text{ V/cm} \hat{z}$.

The goal is to calculate the electric field in the region of beam overlap ($0 \leq \rho \leq 0.15 \text{ cm}$, $3.05 \text{ cm} \leq z \leq 3.35 \text{ cm}$) and determine what percentage of the region satisfied the field homogeneity specifications. In Fig. 8 the shaded area indicates the region where $\vec{E}(\rho, z) = [-19.545 \pm 0.02 \text{ V/cm}] \hat{z}$. The ρ -component of the electric field is extremely small over the entire region, and $|\vec{E}| \approx E_z$. If we assume a uniform atomic beam density, approximately 40% of the atoms in the atomic beam can potentially be excited into a Rydberg state.

V. CONCLUSION

The finite element method is a powerful tool for solving the linear differential equations that appear in electromagnetic theory and quantum mechanics. Section III is sufficiently general and detailed so that the method can easily be implemented by undergraduate or graduate students who

have a basic knowledge of programming. Another important application appropriate for undergraduate quantum mechanics is the solution of the Schrödinger equation in one dimension. Students can solve for bound states and scattering states for arbitrary potentials and explore the physics of systems with more complexity than the square well or the harmonic oscillator. The method is particularly well suited for studying tunneling through nonrectangular barriers. The study of perturbation theory can be enriched by comparing the energy obtained using first-order perturbation theory with the eigenvalue of the exact Hamiltonian computed by the finite element method.

ACKNOWLEDGMENTS

J. Golde received summer support through the Sherman Fairchild Foundation. J. Shertzer is grateful for research funds and student support provided through the Anthony and Renee Marlon Professorship in the Sciences. P. Oxley was funded by the Research Corporation through a Cottrell College Science Award. The authors thank the referees for their insightful comments and helpful suggestions.

- ¹Thomas F. Gallagher, *Rydberg Atoms* (Cambridge University Press, Cambridge, 1994), pp. 27–37, 269–288.
- ²J. C. Day, T. Ehrenreich, S. B. Hansen, E. Horsdal-Pedersen, K. S. Mogensen, and K. Taulbjerg, “Formation of oriented elliptic Rydberg atoms,” *Phys. Rev. Lett.* **72**, 1612–1615 (1994).
- ³K. S. Mogensen, J. C. Day, T. Ehrenreich, E. Horsdal-Pedersen, and K. Taulbjerg, “Coherent elliptic states in lithium,” *Phys. Rev. A* **51**, 4038–4047 (1995).
- ⁴T. Ehrenreich, J. C. Day, S. B. Hansen, E. Horsdal-Pedersen, K. B. MacAdam, and K. S. Mogensen, “Electron capture from oriented elliptic Rydberg atoms,” *J. Phys. B* **27**, L383–L389 (1994).
- ⁵J. C. Day, B. D. DePaola, T. Ehrenreich, S. B. Hansen, E. Horsdal-Pedersen, Y. Leontiev, and K. S. Mogensen, “Electron capture from coherent elliptic Rydberg states,” *Phys. Rev. A* **56**, 4700–4714 (1997).
- ⁶David J. Griffiths, *Introduction to Electrodynamics*, 3rd ed. (Prentice Hall, Upper Saddle River, NJ, 1999), pp. 110–120.
- ⁷Klaus-Jurgen Bathe and Edward L. Wilson, *Numerical Methods in Finite Element Analysis* (Prentice-Hall, Englewood Cliffs, NJ, 1976).
- ⁸David E. Pritchard and Michael P. Bradley, “Atom traps compared with ion traps,” *Phys. Scr.*, T **T59**, 31–33 (1995).
- ⁹L. Ramdas Ram-Mohan, Sunil Saigal, Don Dossa, and J. Shertzer, “The finite element method for energy eigenvalues of quantum mechanical systems,” *Comput. Phys.* **4**, 50–59 (1990).
- ¹⁰L. Ramdas Ram-Mohan, *Finite Element and Boundary Element Applications in Quantum Mechanics* (Oxford University Press, New York, NY, 2002).
- ¹¹George Arfken, *Mathematical Methods for Physicists* (Academic, Orlando, FL, 1985), pp. 573–636.
- ¹²*Handbook of Mathematical Functions*, edited by Milton Abramowitz and Irene Stegun (Dover, New York, 1970), p. 409.